This document is the accepted manuscript version of the following article:
Hawly, T., Johnson, M., Späth, A., Nickles Jäkel, H., Wu, M., Spiecker, E., … Fink, R. H. (2022). Exploring the preparation dependence of crystalline 2D-extended ultrathin C8-BTBT-C8 films. ACS Applied Materials and Interfaces, 14(14), 16830-16838. https://doi.org/10.1021/acsami.2c00097

Exploring the preparation-dependence of crystalline 2D-extended ultrathin C8-BTBT-C8 films

Tim Hawly [a, ‡] *Manuel Johnson* [a, ‡] *Andreas Späth* [a], *Hannah Nickles Jäkel* [a], *Mingjian Wu* [b], *Erdmann Spiecker* [b], *Benjamin Watts* [c], *Alexei Nefedov* [d,†] *and Rainer H. Fink* [a,*]

[a] Friedrich-Alexander-Universität Erlangen-Nürnberg, Department Chemie und Pharmazie, Egerlandstraße 3, 91058 Erlangen, Germany

[b] Friedrich-Alexander-Universität Erlangen-Nürnberg, Institute of Micro- and Nanostructure Research, Cauerstraße 3, 91058 Erlangen, Germany

[c] Paul Scherrer Institute, Villigen 5232, Switzerland

[d] Institute of Functional Interfaces (IFG), Karlsruhe Institute of Technology (KIT), 76344 Eggenstein-Leopoldshafen, Germany.

KEYWORDS. Organic semiconductors, Molecular Self-assembly, Organic thin films, X-ray Microspectroscopy, Electron tomography, 2D nanomaterials.

ABSTRACT. Crystalline organic semiconducting thin films from the benchmark molecule C8-BTBT-C8 were obtained via physical vapor deposition and various solution-based methods. Utilizing atomic force microscopy and X-ray spectromicroscopy, we illustrate the influence of the underlying growth mechanism and determine the highly preparation-dependent orientation of the thiophene backbone. We observe a continuous trend for crystalline C8-BTBT-C8 thin film domains to extend into the mm²-range at near-equilibrium growth conditions. For such well-defined systems, electron diffraction tomography allows to precisely determine the unit cell directly after film deposition and to reveal an 8° molecular tilt angle with respect to the surface normal. This finding is in almost perfect accordance with the values derived from NEXAFS linear dichroism. Within this work, we shine light on both success and challenges connected to the realization of potent, thiophene-based semiconducting films paving the way towards cm²-sized ultrathin organic crystals and their application in organic circuitry.

1. INTRODUCTION. Over the last three decades there has been great scientific interest in small-molecule organic semiconductors (OSCs) particularly due to the possibility of low-cost, large-area production and their compatibility with flexible support materials.[1-3] Nowadays, OSC thin films are commonly used as active layers in organic electronic devices such as light-emitting diodes,[4] organic solar cells,[5] and organic field-effect transistors (OFETs).[6-7] The performance of these devices is decisively influenced by the structural and morphological properties of the organic film. In particular, grain boundaries with interfacial disorder are detrimental to charge transport leading to trap states and ultimately, reducing or limiting the charge carrier mobility.[8-11]

Conventionally, the semiconducting layers are fabricated by physical vapor deposition (thermal evaporation or Knudsen cells). Vacuum sublimation has proven to be advantageous with respect to process control as deposition rate, substrate temperature and nominal film

thickness can be monitored by quartz crystal microbalances (QCM) *in situ.*[12] However, the subsiding, nucleation-based growth mechanism is known to be kinetically limited by (i) the intrinsic sticking coefficient of the molecule to the mostly inorganic substrate and (ii) its temperature-dependent diffusion length.[13-15] Accordingly, research focus within the past 20 years has shifted towards alternative techniques such as spin-coating,[16-20] blade coating,[21] and dip-coating[22-24] that rely on more gradual structure formation in solution.[25] Promoting molecular self-assembly in liquid surroundings,[17, 26] the low-cost fabrication conditions favor well-defined, 2-dimensional (2D) networks of a variety of organic semiconducting compounds. As a result, device parameters (*i.e.*, charge-carrier mobility, drain current, on/off ratio, trap state density) of thus realized OFETs commonly outperform their PVD-processed counterparts by orders in magnitude.[16, 27-29] However, all aforementioned techniques depend on a non-equilibrium process as film formation is limited by the rapidly evaporating solvent and subsequent crystallization on a solid support.[30] Continuous improvement and the pursuit of novel preparation techniques close to the thermodynamic equilibrium is therefore a matter of great significance.

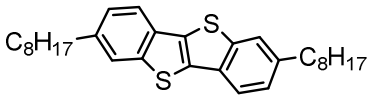

Figure 1. Structural formula of our model substance C8-BTBT-C8.

For the present study, we compare vacuum- and solution-processed specimens of the p-type semiconductor dioctylbenzothienobenzothiophene (C8-BTBT-C8, Figure 1). This compound has already proven to be capable of remarkably high charge-carrier mobilities in various OFET architectures.[16, 31-32] Its status as a benchmark molecule in organic circuitry makes it an ideal candidate to study and illustrate the influence of growth mechanism on the C8-BTBT-C8 microstructure in great detail. In particular, we illustrate and quantify the advantageous effects of film formation taking place under near-equilibrium growth conditions. Being an

underappreciated aspect in previous studies[33], we employ a variety of complementary techniques to investigate and compare key structural properties of solvent-processed C8-BTBT-C8 to samples prepared by vacuum sublimation. We demonstrate the superior crystallinity and domain extension of solution-processed ultrathin films using atomic force microscopy (AFM), selected-area electron diffraction (SAED) and X-ray spectromicroscopy (C-NEXAFS, STXM). We highlight thin-film preparation at the liquid-liquid interface as a yet-to-establish, and highly promising technique towards single-domain layer growth. Our work presents valuable insights and guidance yielding the exact C8-BTBT-C8 unit cell structure derived from electron diffraction tomography (EDT).

2. EXPERIMENTAL SECTION. C8-BTBT-C8 (≥ 99%, HPLC) was purchased from Sigma-Aldrich and used as received. Silicon substrates (p-doped) with a thermally grown, 100-nm-thick silicon oxide layer were provided by Si-Mat (Munich, Germany). For the sake of comparability and regarding potential wettability issues during solution-processing, we did not consider additional substrate modification, *e.g.,* using octadecyltrichlorosilane (OTS) or hexadecyl-trimethoxysilane (HDMS). Despite well-reported benefits to the semiconductor-dielectric interface, we expect considerable limitations regarding the film transfer process from the supporting water surface onto a hydrophobic substrate and subsequently, undesired artefacts within the delicate, ultrathin specimens. Silicon nitride substrates with a membrane thickness of 100 nm for STXM measurements were purchased from Silson Ltd. (United Kingdom). Optical microscopy images were recorded in reflection using a Leica DM 4000M microscope equipped with a Leica DFC320 CCD camera. Film topography and corresponding height profiles were measured in non-contact mode using a JPK NanoWizard 4 AFM. NEXAFS spectra were recorded at the HE-SGM beamline at BESSY II storage ring at the Helmholtz-Zentrum for Materials and Energy (HZB Berlin, Germany). STXM micrographs were taken at the PolLux beamline at the Swiss Light Source (SLS, Villigen, Switzerland).[34-

[35] For electron diffraction tomography (EDT), samples were floated onto water and then carefully transferred onto thin carbon-supported membranes of 200 mesh Cu-based TEM grids and mounted in the Fishione cryo-tomo holder. Experiments were performed on a double Cs-corrected ThermoFisher Scientific Titan Themis3 300 TEM operated at 300 kV. Diffraction data was acquired at liquid nitrogen temperature with the stage continuous tilting typically from -70 to +70 degrees over a period of a few tens of seconds. We have evaluated the critical dose of beam-induced structural degradation to be about 2 $e^-/Å^2$ at room temperature and about 10 $e^-/Å^2$ at liquid nitrogen temperature. Structural degradation seems to be dominated by radiolysis and thus, higher-energy primary beam (300 kV) is advantageous over lower ones (*e.g.* 80 kV). For EDT experiments at liquid nitrogen temperature, total electron fluence of less than 2 $e^-/Å^2$ has been applied and no structural degradation was identified. The EDT data was processed using PETS2 software. Charge-transport characteristics of fabricated OFETs were recorded at a Keithley SCS 4200 parameter analyzer under atmospheric conditions.

Functional organic layers deposited via thermal evaporation were prepared using a home-built vacuum chamber. Deposition of C8-BTBT-C8 onto the heated substrate (T = 333 K) was executed at a working pressure of 10^{-7} mbar with a deposition rate of 0.1 $Ås^{-1}$ and monitored via QCM (Figure 2a) until a nominal thickness of 15 nm was reached. Drop-casted films were fabricated using an air-tight box (Figure 2b). In consideration of solvents with a high vapor pressure, the atmosphere within the setup was allowed to saturate with solvent vapor for five minutes prior to adding the OSC solution droplet. The chamber was connected to adjustable nitrogen gas supply in order to control the solvent vapor concentration and thus evaporation rate during the experiment. A moderate amount of OSC solution (5 - 30 µl) was placed at the top end of a slightly inclined ($3.5° \leq$ substrate tilt $\leq 14°$) 2x1 cm^2 substrate. The box was locked, and the droplet allowed running down the substrate, which led to thin-film precipitation. This method provides film-forming conditions in the trailing edge of the droplet that are similar to

blade-coating.[36] For films prepared at the liquid-liquid interface, beakers were cleaned by sonication in acetone and isopropanol for 15 minutes subsequently and rinsed thoroughly with deionized water afterwards. 15 ml of Millipore water were then given into the beaker and OSC solution (50 – 400 µl) was added dropwise to form a floating lens on the water surface. Beakers were stored at 280 K until the solvent had evaporated. Resulting thin films were transferred from the water surface onto silicon wafers using a custom-built vertical lifting system at a constant speed of approximately 0.5 mm/s (Figure 2c).

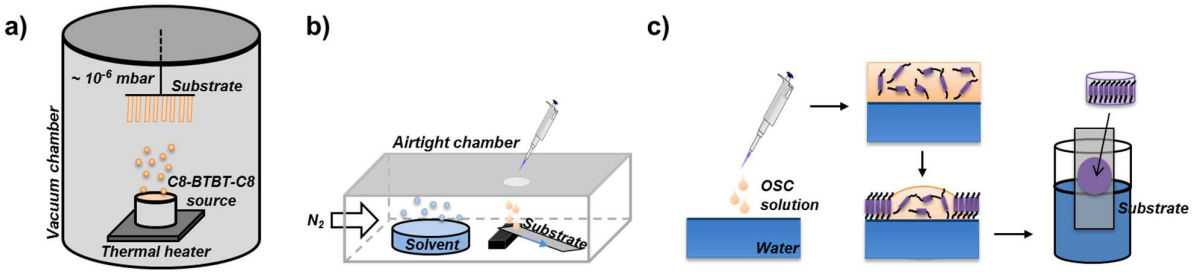

Figure 2. Fabrication processes for C8-BTBT-C8 thin films, (a) thermal evaporation in vacuo, (b) drop-casting within a solvent-saturated atmosphere on an inclined substrate, (c) thin-film preparation at the liquid-liquid interface.

30 nm thick gold source and drain contacts for OFETs were evaporated using a conventional shadow mask containing various transistor geometries W/L (300/20 µm, 450/30 µm, 600/40 µm) at a working pressure of 10^{-6} mbar and with a deposition rate of 0.3 $Å s^{-1}$. Extracted charge-carrier characteristics are summarized in Table 1. The authors would like to point out that in all respects, solvent-prepared films exhibit better performance compared to vacuum-processed BTBT films. Parameters do not yet compare with benchmark architectures reported in literature (μ = 43 cm^2/Vs, $I_{On}/I_{Off} > 10^7$)[16, 37] due to imperfect device engineering in our case.

Table 1: IV parameters for manufactured top-contact bottom-gate OFET structures including maximum and average hole mobilities, on/off-ratios, average trap state densities and threshold voltages (see S1 for further information). Average values are deduced from a minimum of five individual devices.

Preparation	μ_{max}	μ_{avg}	$\left(\frac{I_{On}}{I_{Off}}\right)_{max}$	$\left(\frac{I_{On}}{I_{Off}}\right)_{avg}$	(TSD_{avg})	$-(V_{Th})_{avg}$
	cm²/Vs				*cm^{-2}/eV^{-1}*	*V*
Vacuum dep.	1.46	1.36	4.6 x 10^5	3.2 x 10^5	1.1 x 10^{13}	14.4
Drop-cast.	3.59	2.05	9.6 x 10^6	6.7 x 10^6	7.1 x 10^{12}	16.5
Liq.-liq.	2.89	1.49	2.3 x 10^6	1.0 x 10^6	7.0 x 10^{12}	17.7

3. RESULTS AND DISCUSSION. It is common knowledge that the substrate surface has significant impact on the early stages of organic film growth from PVD in vacuum. Competitive interactions are decisive for the growth modes, *i.e.*, stronger intermolecular interactions will favor island growth while substrate-related influences (interfacial interactions) affect diffusion lengths and thus initial nucleation density,[38] but also the molecular configuration.[39] Therefore, judgement of the characteristic growth behavior can hardly take place using an interacting support, such as highly oriented pyrolytic graphite (HOPG) or metal surfaces, and an inert substrate is preferred. Hence, thermally evaporated C8-BTBT-C8 thin films with a nominal thickness of 15 nm on thermally grown SiO_2 will be considered as reference samples from here on.

3.1 THERMAL EVAPORATION. Figure 3a shows the thin-film morphology of evaporated C8-BTBT-C8/SiO_2 probed by non-contact AFM. We observe rather dense island structures with an average step height of 3.73 nm (from 30 single measurements)

corresponding to the molecular long *c*-axis[32, 40] within the upmost layers. This suggests that the C8-BTBT-C8 molecules tend to adopt an upright conformation. Clearly, nucleation is a common occurrence as multiple small-area molecular clusters form on top of non-closed subjacent layers. Hence, we consider C8-BTBT-C8 to follow the Volmer-Weber growth mode upon *in vacuo* deposition on SiO_2 with the molecule-molecule interaction being stronger than the molecule-substrate interaction.

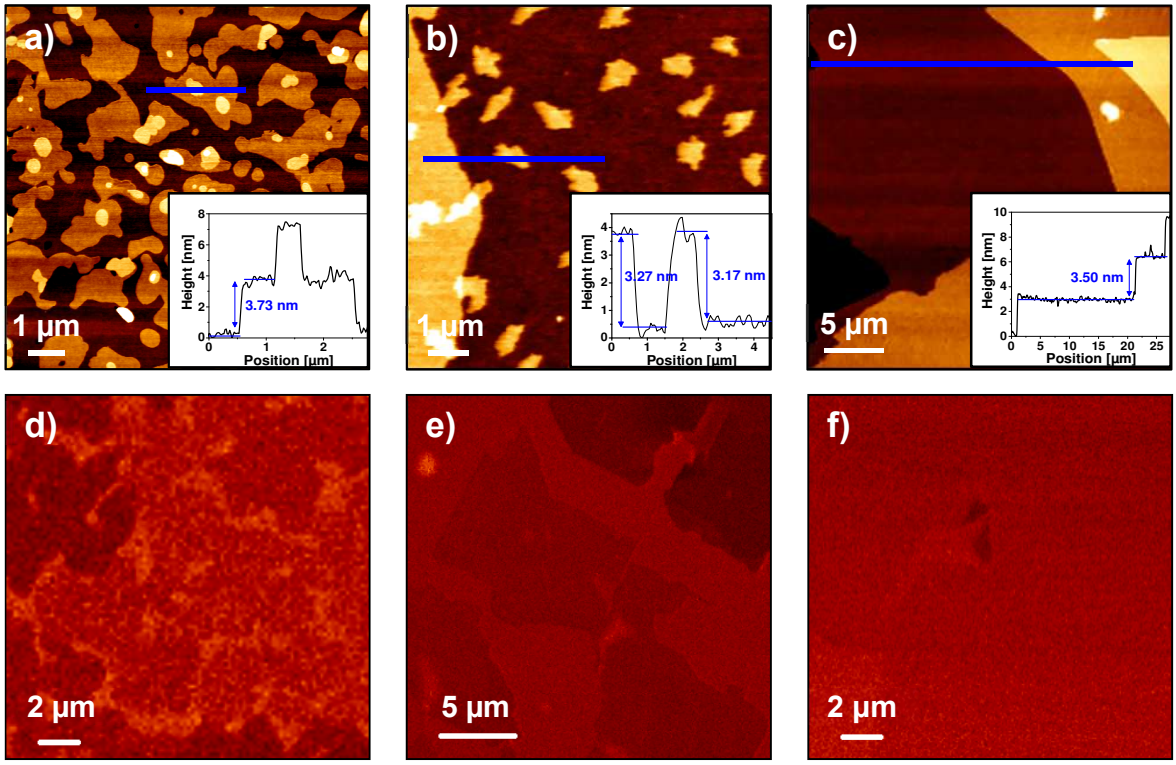

Figure 3. AFM images with corresponding height profiles (top) of C8-BTBT-C8 thin films fabricated via (a) thermal evaporation, (b) drop-casting and (c) liquid-liquid processing. Respective STXM micrographs were recorded at resonant energies, *i.e.*, 285.5 eV (thermal evaporation, Figure. 3d), 285.1 eV (drop-casting, Figure. 3e) and 284.8 eV (liquid-liquid, Figure. 3f), and thickness-corrected afterwards. Hence, all emerging contrast is based on varying molecular orientation within the sample (see S3 for further information).

It has been reported earlier that independently growing islands coalesce in the early stage of film growth.[41] Indeed, molecular-orientation contrast in STXM (Figure 3d) reveals that the microstructure is dominated by azimuthally rotated domains with numerous internal grain boundaries due to excessive nucleation and limited molecular diffusion. This results in an inhomogeneous, polycrystalline microstructure and consequently, the performance of such thermally evaporated films in an electronic device is decisively limited (see Table 1 and S1-1 for further information) as charge transport ideally occurs through single-crystalline junctions at the C8-BTBT-C8/SiO_2 interface. It is noted that the nucleation density during growth process can be lowered by the careful adjustment of process parameters such as substrate temperature and deposition rate. Still, the intrinsic, diffusion-limited mechanism promotes film formation at non-equilibrium conditions and thereby produces a well-defined 2D extended homogeneous film.

3.2 DROP-CASTING. In a first step away from nucleation-dominated film growth *in vacuo*, we realized few-layer systems of C8-BTBT-C8 via a modified drop-casting approach according to Figure 2b. Films with an overall thickness around 30 nm precipitate readily from a 0.3 mg/ml chloroform solution. Their morphology is defined by 2D-extended organic thin-film sheets with an average step height of 3.27 nm (from 30 single measurements). In addition, regularly occurring agglomerates with a lateral extension of 1-2 µm and an average step height of 3.17 nm are observed via AFM (Figure 3b). Hence, both structural motifs exhibit step heights in the range of the C8-BTBT-C8 molecular long axis. In general, larger substrate tilt angles during preparation are favorable as the solution contact line recedes faster towards the lower end of the substrate. Molecules are thus given a smaller amount of time to precipitate yielding thinner and more homogeneous structures (Figure S4).

Clear improvements as compared to vacuum-processed films are confirmed as the dimensions of the underlying domains excel their evaporated counterparts by several tens of

micrometers. Expectedly, the mobility of the dissolved molecules is higher leading to favorable intermolecular interaction during the growth process with precipitation on top of existing layers becoming a less likely process. This is confirmed by STXM images (Figure 3e) as homogeneous arrays with clear, crystalline edges are observed illustrating the inherently different growth mechanism. The true expanse of these well-defined structures can only be assumed as they exceed the scan range. The influence of structural imperfections of the underlying substrate is decisively lower as compared to evaporated thin films. Hence, such layered structures provide a vastly superior structure and improved crystallinity in terms of long-range molecular order and internal homogeneity with fewer domain defects.

However, drop-casting, as conducted within this approach, still depicts a non-equilibrium process. While the time provided for molecular self-assembly (determined by the evaporation of the used solvent) increases as compared to vacuum-deposited structures, film formation is still 'quenched' by the rather rapidly receding contact line. Upon complete solvent evaporation, we expect this to lead to agglomerates, which are sporadically observed on top of the extended, smooth structures in AFM micrographs (Figure 3b). Accordingly, isolated bright spots can also be found in the corresponding STXM image representing a varying molecular orientation within these sections.

3.3 LIQUID-LIQUID INTERFACE. In order to achieve film formation in near-equilibrium conditions and to eliminate all unfavorable substrate contributions, we focus on a solution-based method initially introduced by Hu *et al.*[33] Here, intermolecular interactions such as π-π stacking and van-der-Waals (VdW) interactions between the building blocks of C8-BTBT-C8 are emphasized within steady liquid surroundings leading to largely extended, defect-free single crystalline films. Conveniently, the water surface acts as a defect-free substrate during film formation and the moderately evaporating solvent provides a perfect environment for molecular diffusion and subsequent self-organization. It is not expected to

observe an intrinsic diffusion limit during the growth process, which depicts another decisive advantage, especially with respect to vapor growth in vacuo.

C8-BTBT-C8 thin films were prepared at the water-solvent interface based on original solutions from chloroform, toluene and chloroform-toluene mixtures. It should be noted that two prerequisites for successful film growth at the liquid-liquid interface are that (i) the solvent has a lower density than water and (ii) the evaporation rate of the solvent gives the C8-BTBT-C8 molecules an appropriate amount of time to self-assemble. The nature of the (co-)solvent is also known to play a key role in film formation.[33, 42-43] Especially toluene, being an aromatic compound and capable of pi-pi interactions, is expected to act as a mediator within the highly diluted solution promoting attractive intermolecular interactions between the core units of C8-BTBT-C8 molecules. Additionally, the vapor pressure of toluene (13.7 hPa) during film growth at 280 K is significantly lower than for chloroform (113.5 hPa), which benefits the self-assembly process in solution in mixtures of both solvents (Figure S9).

Microscopically, we observe widespread, molecularly flat C8-BTBT-C8 domains with average step heights of 3.50 nm (from 30 single measurements, Figure 3c) according to the *c* extension of the molecule within the error margin of the AFM experiment.[44-46] The lateral dimension of such continuous sheets exceeds island structures grown *in vacuo* to a great extent while exhibiting a decisively lower amount of excess material, i.e., potential nucleation centers, compared to drop-cast specimens (Figure 3b). Hence, non-contact AFM measurements confirm superior film morphology as well as favorable layered growth compared to both vacuum-processed and drop-casted samples. Also, corresponding STXM images (Figure 3f) show practically no molecular orientation contrast, meaning that such layered systems should possess superior crystallinity and accordingly, the overall number of domain boundaries is expected to be considerably lower.

Over time, we notice crevices corresponding to the step height of monolayers in formerly smooth, flat structures (Figure 4d). We explain these undesired aging effects by the local enrichment of solvent molecules, in this case toluene, between the C8-BTBT-C8 core units via attractive π-π interactions. They are expected to be capable of withstanding the gradual evaporation process in the highly diluted original solution at 280 K. After a given amount of time under atmospheric conditions, the solvent evaporates resulting in undesired voids within the layered microstructure. This phenomenon is also observable with the use of other common aromatic solvents exhibiting even lower vapor pressures, *e.g.*, halogenated benzene derivatives.

It is noted that such aging effects are not observed once *n*-alkanes such as hexane or heptane (liquid-liquid processing) or chloroform (drop-casting) are used, as these solvents are not capable of attractively interacting with the C8-BTBT-C8 core units but only to lower degree with the symmetrically attached octyl chains (Figure S10). This illustrates that the reproducible realization of single-crystalline structures requires careful optimization, especially regarding the manifold processing parameters such as solvent, concentration, droplet volume, evaporation rate and temperature.

Conclusions regarding the molecular conformation of the C8-BTBT-C8 layers are confirmed via angle dependent NEXAFS measurements at the carbon K-edge (Figure 4a). In general, the obtained angle-dependent spectra show the characteristic C8-BTBT-C8 fingerprint, *i.e.*, we assign the sharp transitions near 285 eV to the prominent C1s→π*(C=C) resonance of the aromatic BTBT core unit.[47] Spectral features at 288 eV are attributed to C1s→σ*(C-H) and C1s→π*(C=C) transitions.[47-49] Broad-shaped peaks from 294 eV refer to C1s→σ*(C-C, C=C) transitions of aromatic core unit and alkyl chains.[48] In the case of a preferred molecular orientation, the absorption intensity varies for both resonant C1s→π* and C1s→σ* transitions upon change of the electric field vector of the polarized X-ray beam (NEXAFS linear dichroism effect).[50]

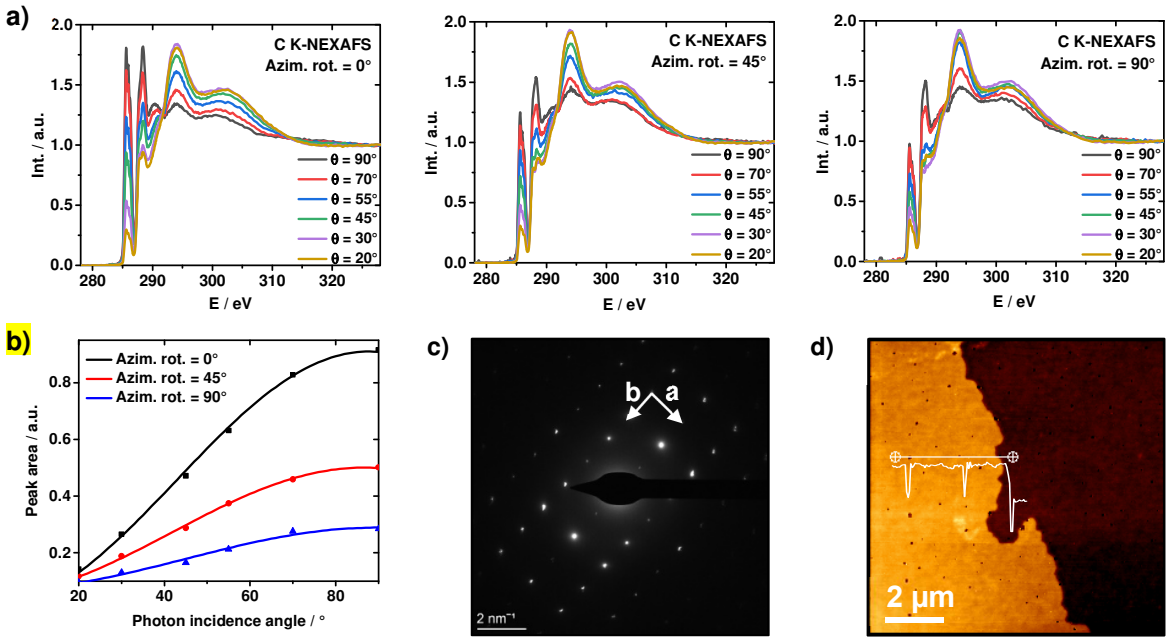

Figure 4. Characterization of representative C8-BTBT-C8 thin films from liquid-liquid processing. (a) Angle dependent NEXAFS spectra at three different azimuthal rotations of the sample, (b) corresponding derivation of the core unit tilt angle, (c) Selected-area electron diffraction pattern with indicated axes of the unit cell, (d) AFM micrograph of a liquid-liquid processed film after four days under atmospheric conditions. Aging-related vacancies in the denoted height profile correspond to 3.01 nm, 3.08 nm and 2.95 nm (from left to right).

Qualitatively, a distinct molecular arrangement within the film is observed irrespective of the fabrication method (Figure S12-14). For highly aligned structures, as observed via AFM and STXM, the significant part of the absorbed intensity is described by (1).

$$I_v^{\parallel} = cos^2\theta cos^2\alpha + sin^2\theta sin^2\alpha cos^2\phi \qquad (1)$$

where θ is the experimental photon incidence angle, α is the polar angle between the surface normal and the π* orbitals perpendicular to the aromatic core unit and ϕ is the orbital azimuthal angle depending on the sample rotation with respect to the electric field vector $\vec{E}$ of the incident photon beam.[50] At large photon incidence angles (θ = 90°), π* transitions at approximately 285 eV are of strong intensity and σ* transitions from 294 eV decrease in intensity with the

opposite behavior occurring at small incidence angles (θ = 20°, Figure 4a). This is indicative of the molecular tilt angle, $\beta = 90° - \alpha$, being smaller than 35.3° (NEXAFS "magic" angle). While numerous appropriate fitting procedures are well reported in literature,[48, 50-51] the approach first introduced by Zheng *et al.* is used herein to determine the accurate orientation of the core unit according to

$$\frac{I_v(\theta)}{I_v(\theta = 90°)} = 1 + P \times \left(\frac{2}{sin^2\alpha} - 3\right) \times cos^2\theta \qquad (2)^{52}$$

P = 0.91 is the degree of polarization depending on the instrument. The derived molecular orientation parameters for the different preparation techniques are listed in Table 2 (see S6 for further information).

The data show distinct polar (intensity difference between resonant transitions within one spectrum) and azimuthal anisotropy (overall intensity difference between three different sample orientations) for drop-cast (Figure S13) and liquid-liquid processed films (Figure 4a, S14). In contrast to vacuum-processed films, which exhibit isotropic growth behavior resulting in numerous azimuthally rotated domains, we are able to extract a distinct azimuthal angle, ϕ (in addition to the average polar angle, α) for solution-processed specimens. This confirms the large degree of molecular order, a close-to-upright orientation of the C8-BTBT-C8 molecule (the π* signal is strongest at normal incidence), an in-plane crystal alignment and hence, superior thin-film quality. It is noted that obtained values and error margins for the azimuthal orientation (Table 2) crucially depend on the large-area homogeneity of the specimen. Drop-casted films were prepared using a tilted substrate, *i.e.*, they exhibit a preferred growth direction, and also, structures commonly cover the 1.2 x 0.5 mm² spot size even upon sample rotation during the NEXAFS experiment. In contrast, it seems likely that singular clusters on top of liquid-liquid processed samples as well as flake boundaries or uncovered substrate sections may contribute to locally inhomogeneous azimuthal orientation leading to larger deviation from an ideal fit (see S6-3 and S6-4 for further information).

The derived molecular tilt angles, β, (Figure 4b, Table 2) are in good accordance with solution-processed systems reported by Watanuki *et al.* [48] Interestingly, β is considerably smaller for solution-processed specimen accounting for a more upright standing configuration. This is expected to benefit charge-transport characteristics of the semiconductor (Table 1) as a 'vertical' orientation of the core also indicates increased orbital overlap.[53] It is noted that the derived values do not take the orientation of the symmetrically attached octyl chains into account which, in any case, are expected to be susceptible to vibrational motion in the condensed phase.[54]

The exceptional crystallinity of the C8-BTBT-C8 layers prepared by the liquid-liquid approach is illustrated by SAED experiments (Figure 4c). In general, we observe an unambiguous electron diffraction pattern indicative of an oriented and highly periodic arrangement with lattice parameters (a = 5.91 Å, b = 7.57 Å) being in good accordance with the previously reported bulk structure of the compound.[44, 46] The b axis shows to be slightly shorter than for the bulk structure (7.88 Å)[55] as well as for other solution-processed specimen (7.8-8.1 Å.).[45, 56] Accordingly, the molecules are packed denser within the crystal, which is expected to benefit charge-transport related performance data due to improved orbital overlap. This confirms the favorable conditions for film growth at the molecularly flat, defect-free liquid-liquid interface regarding ultrathin, extended and well-defined films as compared to conventional diffusion-controlled growth *in vacuo*. The intermolecular interactions are dominated by herringbone-type CH-π interactions, S-S interaction, and hydrophobic interaction between the octyl chains.[55] It is noted that the systematic absence of Bragg spots at *h,0* (*h* odd) and *0,k* (*k* odd) depicts forbidden reflections due to the reported herringbone crystal structure of the compound.[57-58]

Table 2. Orientation parameters of the C8-BTBT-C8 core unit depending on the fabrication process from NEXAFS analysis. Note, that the ϕ-values (azimuthal domain rotation) depend on the sample mounting and must not be compared for the different preparations yielding anisotropic orientations.

	α	**β**	**ϕ**
Thermal evaporation	77° ± 3°	13° ± 3°	isotropic
Drop-casting	86° ± 3°	4° ± 3°	66.3°± 8°
Liquid-liquid	84° ± 3°	6° ± 3°	24.1°± 12°

A well-defined, liquid-liquid processed C8-BTBT-C8 few-layer sample has been selected for unit cell structure determination using EDT. Since the *c*-axis of the unit cell of BTBT family crystals is contained within the π-plane, and the sample transfer is not expected to change the orientation relationship of the 2D crystallite unit cells with respect to the substrate, *i.e.*, the TEM grid, the EDT measured unit cell orientation provides an unambiguous determination of the π-plane orientation (Figure 5).

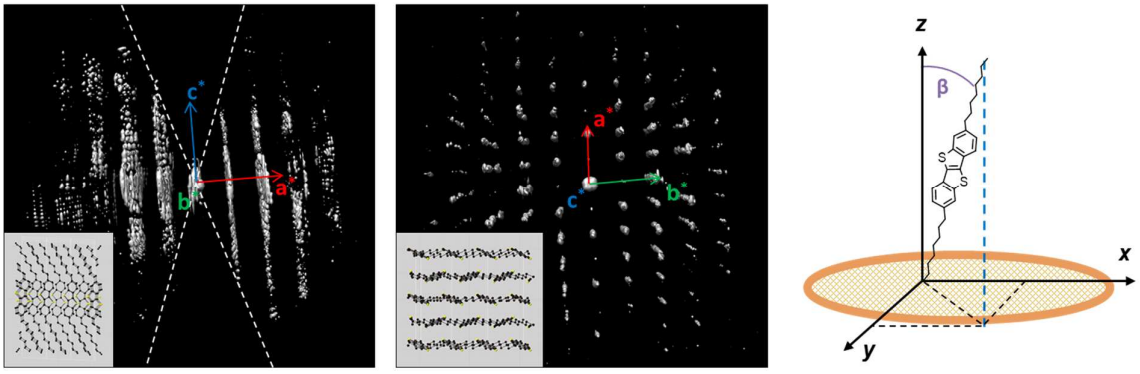

Figure 5: Perspective views of the EDT data and the unit cell representations (insets) and scheme of deriving the molecule inclination angle using the measured orientation matrix. The reciprocal lattice is shown along b* (left) and c* direction (middle), respectively. Based on the measured orientation matrix of reciprocal basis vectors, the real space orientation matrix Eq.

(3) as well the unit cell c-axis orientation can be easily calculated which coincides with the molecular tilt from the surface normal. See Supplementary information for further information, frame-by-frame visualization of the rotation process and holistic unit cell representation.

The extracted unit cell parameters are $a = 5.91$ Å, $b = 7.57$ Å, $c = 28.95$ Å, $\alpha = 90°$, $\beta = 90.64^0$ and $\gamma = 90°$, which is very close to literature values of the bulk material.[55] The directly measured orientation matrix quantitatively describes the orientation of the reciprocal basis vectors with respect to electron beam direction at zero-degree stage tilt, *i.e.*, surface normal of the sample. Using the reciprocal relationship, the orientation matrix of real-space unit cell basis can be calculated to be

$$\begin{bmatrix} a_x & b_x & c_x \\ a_y & b_y & c_y \\ a_z & b_z & c_z \end{bmatrix} = \begin{bmatrix} 0.3574 & -7.4895 & 4.00819 \\ 5.9019 & 0.4660 & -0.4256 \\ -0.07178 & 1.0510 & 28.6661 \end{bmatrix} \qquad (3)$$

The *c*-axis orientation with respect to the surface normal is calculated to be 8° from eq. (4).

$$\beta = tan^{-1} \sqrt{c_x^2 + c_y^2} \Big/ c_z^2 \qquad (4)$$

This indicates that the molecular long axis is inclined $\beta = 8°$ from the surface normal (Figure 5) confirming the tilt angle derived via angle-dependent NEXAFS measurements within the experiment uncertainty of ± 3° (see Table 2). It is noted that even directly after film deposition onto the TEM grid and at experimental temperatures around 100 K, no ice formation within the sample was observed during the measurement. Hence, in addition to the exceptional in-plane crystallinity and structure elucidation, we are also able to emphasize the excellent suitability of the water surface as a very beneficial substrate for organic film growth.

4. CONCLUSIONS. In summary, we have successfully realized well-defined C8-BTBT-C8 thin films from vacuum sublimation, a slightly modified drop-casting approach and solution processing at the liquid-liquid interface. We are able to illustrate (i) the unbeneficial influence

of

non-equilibrium conditions *in vacuo* leading to Volmer-Weber growth and (ii) the superior, layered 2D structure of various solution-processed specimens. With increasing time in liquid surroundings, *i.e.*, close to thermodynamic equilibrium, we observe significantly improving long-range molecular order. Distinct azimuthal anisotropy within drop-cast and liquid-liquid processed specimens was confirmed by angle-dependent NEXAFS spectroscopy underlining the significantly larger 2D extension of uniform domains. For the solvent-prepared specimens we deduce a lower average molecular tilt angle than for vacuum-processed films, which is known to benefit charge-transport characteristics. Utilizing EDT as a complimentary technique, we were able to verify the overall molecular orientation and, in addition, yield an unprecedented and precise representation of the neat molecular alignment in liquid-liquid grown 2D single crystals. While we can report the lack of interstitial water molecules in the structures, the partial inclusion of aromatic solvent molecules is also assumed from aged samples. Satisfyingly, our studies do not suggest an intrinsic limit in domain size regarding single-domain growth at near-equilibrium conditions. This implies applicability to a wide range of similar small-molecule semiconductors paving the way towards well-defined, cm^2-sized, ultrathin crystals.

ASSOCIATED CONTENT

Supporting Information.

S1: Charge-transport parameters of fabricated C8-BTBT-C8 OFETs.

S2: Influence of varying substrate inclination angles on the thin-film morphology.

S3: Scanning transmission X-ray microscopy.

S4: Solvent dependence for liquid-liquid processed C8-BTBT-C8 thin films.

S5: AFM images of aged toluene and heptane-based C8-BTBT-C8 thin films.

S6: NEXAFS fitting procedure and tilt angle derivation for fabricated thin films.

Supplementary information for this article is available.

AUTHOR INFORMATION

Corresponding Author

*Rainer H. Fink, Friedrich-Alexander-Universität Erlangen-Nürnberg, Department Chemie und Pharmazie, Egerlandstraße 3, 91058 Erlangen, Germany, E-mail: rainer.fink@fau.de

Present Addresses

† Alexei Nefedov, Institute of Functional Interfaces (IFG), Karlsruhe Institute of Technology (KIT), 76344 Eggenstein-Leopoldshafen, Germany.

Author Contributions

‡T.H. and M.J. contributed equally to this work.

Funding Sources:

TH, MJ, MW, and ES received financial support from the German Research Foundation via the Research Training Group GRK 1896 "*In situ* microscopy with electrons, X-rays and scanning probes". AS, NHJ, and RHF obtained funding from the Federal Ministry of Education and Research (BMBF project number 05K19WE2). The project was partly supported by the "SolTech – Solar Technologies goes hybrid" initiative by the State of Bavaria.

Notes

The authors declare no competing financial interest.

ACKNOWLEDGMENT

The Helmholtz Zentrum Berlin für Materialien und Energie (HZB) is gratefully acknowledged for beamtime allocation, technical assistance and travelling support. The authors would like to thank Dr. Ole Lytken (FAU) for assistance in quantitative NEXAFS data analysis. The authors thank the Swiss Light Source for beamtime at PolLux. The PolLux end station was financed by the German Ministerium für Bildung und Forschung (BMBF) through contracts 05K16WED and 05K19WE2.

REFERENCES

1. Kumar, B.; Kaushik, B. K.; Negi, Y. S., Organic Thin Film Transistors: Structures, Models, Materials, Fabrication, and Applications: A Review. *Polymer Reviews* **2014,** *54* (1), 33-111.
2. Diao, Y.; Tee, B. C. K.; Giri, G.; Xu, J.; Kim, D. H.; Becerril, H. A.; Stoltenberg, R. M.; Lee, T. H.; Xue, G.; Mannsfeld, S. C. B.; Bao, Z., Solution coating of large-area organic semiconductor thin films with aligned single-crystalline domains. *Nature Materials* **2013,** *12* (7), 665-671.
3. Mas-Torrent, M.; Masirek, S.; Hadley, P.; Crivillers, N.; Oxtoby, N. S.; Reuter, P.; Veciana, J.; Rovira, C.; Tracz, A., Organic field-effect transistors (OFETs) of highly oriented films of dithiophene-tetrathiafulvalene prepared by zone casting. *Org. Electron.* **2008,** *9* (1), 143-148.
4. Lee, S.; Kwon, J. H.; Kwon, S.; Choi, K. C., A Review of Flexible OLEDs Toward Highly Durable Unusual Displays. *IEEE Transactions on Electron Devices* **2017,** *64* (5), 1922-1931.
5. Kaur, N.; Singh, M.; Pathak, D.; Wagner, T.; Nunzi, J. M., Organic materials for photovoltaic applications: Review and mechanism. *Synth. Met.* **2014,** *190*, 20-26.
6. Surya, S. G.; Raval, H. N.; Ahmad, R.; Sonar, P.; Salama, K. N.; Rao, V. R., Organic field effect transistors (OFETs) in environmental sensing and health monitoring: A review. *TrAC, Trends Anal. Chem.* **2019,** *111*, 27-36.
7. Di, C.-a.; Zhang, F.; Zhu, D., Multi-Functional Integration of Organic Field-Effect Transistors (OFETs): Advances and Perspectives. *Adv. Mater.* **2013,** *25* (3), 313-330.
8. Halik, M.; Klauk, H.; Zschieschang, U.; Schmid, G.; Ponomarenko, S.; Kirchmeyer, S.; Weber, W., Relationship between molecular structure and electrical performance of oligothiophene organic thin film transistors. *Advanced Materials* **2003,** *15* (11), 917-922.
9. Horowitz, G., Tunneling Current in Polycrystalline Organic Thin-Film Transistors. *Advanced Functional Materials* **2003,** *13* (1), 53-60.
10. Mas-Torrent, M.; Rovira, C., Role of Molecular Order and Solid-State Structure in Organic Field-Effect Transistors. *Chem. Rev.* **2011,** *111* (8), 4833-4856.

11. Don Park, Y.; Lim, J. A.; Lee, H. S.; Cho, K., Interface engineering in organic transistors. *Mater. Today* **2007,** *10* (3), 46-54.
12. Hill, I. G.; Milliron, D.; Schwartz, J.; Kahn, A., Organic semiconductor interfaces: electronic structure and transport properties. *Appl. Surf. Sci.* **2000,** *166* (1), 354-362.
13. Mukherjee, S.; Zhou, C. M.; Gall, D., Temperature-induced chaos during nanorod growth by physical vapor deposition. *J. Appl. Phys.* **2009,** *105* (9), 094318.
14. Kloc, C.; Simpkins, P. G.; Siegrist, T.; Laudise, R. A., Physical vapor growth of centimeter-sized crystals of α-hexathiophene. *J. Cryst. Growth* **1997,** *182* (3), 416-427.
15. Kubono, A.; Akiyama, R., Orientational Mechanism for Long-Chain Organic Molecules During Physical Vapor Deposition. *Molecular Crystals and Liquid Crystals* **2002,** *378* (1), 167-183.
16. Yuan, Y.; Giri, G.; Ayzner, A. L.; Zoombelt, A. P.; Mannsfeld, S. C. B.; Chen, J.; Nordlund, D.; Toney, M. F.; Huang, J.; Bao, Z., Ultra-high mobility transparent organic thin film transistors grown by an off-centre spin-coating method. *Nature Communications* **2014,** *5*, 3005.
17. Zhang, F.; Di, C.-a.; Berdunov, N.; Hu, Y.; Hu, Y.; Gao, X.; Meng, Q.; Sirringhaus, H.; Zhu, D., Ultrathin Film Organic Transistors: Precise Control of Semiconductor Thickness via Spin-Coating. *Adv. Mater.* **2013,** *25* (10), 1401-1407.
18. Mitzi, D. B.; Kosbar, L. L.; Murray, C. E.; Copel, M.; Afzali, A., High-mobility ultrathin semiconducting films prepared by spin coating. *Nature* **2004,** *428* (6980), 299-303.
19. Chang, C.-C.; Pai, C.-L.; Chen, W.-C.; Jenekhe, S. A., Spin coating of conjugated polymers for electronic and optoelectronic applications. *Thin Solid Films* **2005,** *479* (1), 254-260.
20. Dai, F.; Liu, X.; Yang, T.; Qian, J.; Li, Y.; Gao, Y.; Xiong, P.; Ou, H.; Wu, J.; Kanehara, M.; Minari, T.; Liu, C., Fabrication of Two-Dimensional Crystalline Organic Films by Tilted Spin Coating for High-Performance Organic Field-Effect Transistors. *ACS Applied Materials & Interfaces* **2019,** *11* (7), 7226-7234.
21. Niazi, M. R.; Li, R.; Qiang Li, E.; Kirmani, A. R.; Abdelsamie, M.; Wang, Q.; Pan, W.; Payne, M. M.; Anthony, J. E.; Smilgies, D.-M.; Thoroddsen, S. T.; Giannelis, E. P.; Amassian, A., Solution-printed organic semiconductor blends exhibiting transport properties on par with single crystals. *Nature Communications* **2015,** *6* (1), 8598.
22. Li, M.; An, C.; Pisula, W.; Müllen, K., Alignment of Organic Semiconductor Microstripes by Two-Phase Dip-Coating. *Small* **2014,** *10* (10), 1926-1931.
23. Wu, K.; Li, H.; Li, L.; Zhang, S.; Chen, X.; Xu, Z.; Zhang, X.; Hu, W.; Chi, L.; Gao, X.; Meng, Y., Controlled Growth of Ultrathin Film of Organic Semiconductors by Balancing the Competitive Processes in Dip-Coating for Organic Transistors. *Langmuir* **2016,** *32* (25), 6246-6254.
24. Jang, J.; Nam, S.; Im, K.; Hur, J.; Cha, S. N.; Kim, J.; Son, H. B.; Suh, H.; Loth, M. A.; Anthony, J. E.; Park, J.-J.; Park, C. E.; Kim, J. M.; Kim, K., Highly Crystalline Soluble Acene Crystal Arrays for Organic Transistors: Mechanism of Crystal Growth During Dip-Coating. *Adv. Funct. Mater.* **2012,** *22* (5), 1005-1014.
25. Yu, P.; Zhen, Y.; Dong, H.; Hu, W., Crystal Engineering of Organic Optoelectronic Materials. *Chem* **2019,** *5* (11), 2814-2853.

26. Norrman, K.; Ghanbari-Siahkali, A.; Larsen, N. B., 6 Studies of spin-coated polymer films. *Annual Reports Section "C" (Physical Chemistry)* **2005,** *101* (0), 174-201.
27. Wang, Q.; Juarez-Perez, E. J.; Jiang, S.; Qiu, L.; Ono, L. K.; Sasaki, T.; Wang, X.; Shi, Y.; Zheng, Y.; Qi, Y.; Li, Y., Spin-Coated Crystalline Molecular Monolayers for Performance Enhancement in Organic Field-Effect Transistors. *The Journal of Physical Chemistry Letters* **2018,** *9* (6), 1318-1323.
28. Minari, T.; Darmawan, P.; Liu, C.; Li, Y.; Xu, Y.; Tsukagoshi, K., Highly enhanced charge injection in thienoacene-based organic field-effect transistors with chemically doped contact. *Appl. Phys. Lett.* **2012,** *100* (9), 093303.
29. Darmawan, P.; Minari, T.; Xu, Y.; Li, S.-L.; Song, H.; Chan, M.; Tsukagoshi, K., Optimal Structure for High-Performance and Low-Contact-Resistance Organic Field-Effect Transistors Using Contact-Doped Coplanar and Pseudo-Staggered Device Architectures. *Adv. Funct. Mater.* **2012,** *22* (21), 4577-4583.
30. Pichumani, M.; Bagheri, P.; Poduska, K. M.; González-Viñas, W.; Yethiraj, A., Dynamics, crystallization and structures in colloid spin coating. *Soft Matter* **2013,** *9* (12), 3220-3229.
31. Minemawari, H.; Yamada, T.; Matsui, H.; Tsutsumi, J.; Haas, S.; Chiba, R.; Kumai, R.; Hasegawa, T., Inkjet printing of single-crystal films. *Nature* **2011,** *475* (7356), 364-7.
32. Janneck, R.; Pilet, N.; Bommanaboyena, S. P.; Watts, B.; Heremans, P.; Genoe, J.; Rolin, C., Highly Crystalline C8-BTBT Thin-Film Transistors by Lateral Homo-Epitaxial Growth on Printed Templates. *Adv. Mater.* **2017,** *29* (44), 1703864.
33. Xu, C.; He, P.; Liu, J.; Cui, A.; Dong, H.; Zhen, Y.; Chen, W.; Hu, W., A General Method for Growing Two-Dimensional Crystals of Organic Semiconductors by "Solution Epitaxy". *Angew. Chem. Int. Ed. Engl.* **2016,** *55* (33), 9519-23.
34. Frommherz, U.; Raabe, J.; Watts, B.; Stefani, R.; Ellenberger, U., Higher Order Suppressor (HOS) for the PolLux Microspectroscope Beamline at the Swiss Light Source SLS. *AIP Conference Proceedings* **2010,** *1234* (1), 429-432.
35. Raabe, J.; Tzvetkov, G.; Flechsig, U.; Böge, M.; Jaggi, A.; Sarafimov, B.; Vernooij, M. G. C.; Huthwelker, T.; Ade, H.; Kilcoyne, D.; Tyliszczak, T.; Fink, R. H.; Quitmann, C., PolLux: A new facility for soft x-ray spectromicroscopy at the Swiss Light Source. *Rev. Sci. Instrum.* **2008,** *79* (11), 113704.
36. Ding, L.; Zhao, J.; Huang, Y.; Tang, W.; Chen, S.; Guo, X., Flexible-Blade Coating of Small Molecule Organic Semiconductor for Low Voltage Organic Field Effect Transistor. *IEEE Electron Device Letters* **2017,** *38* (3), 338-340.
37. He, D.; Qiao, J.; Zhang, L.; Wang, J.; Lan, T.; Qian, J.; Li, Y.; Shi, Y.; Chai, Y.; Lan, W.; Ono, L. K.; Qi, Y.; Xu, J.-B.; Ji, W.; Wang, X., Ultrahigh mobility and efficient charge injection in monolayer organic thin-film transistors on boron nitride. *Science Advances* **2017,** *3* (9), e1701186.
38. Meyer zu Heringdorf, F.-J.; Reuter, M. C.; Tromp, R. M., Growth dynamics of pentacene thin films. *Nature* **2001,** *412* (6846), 517-520.
39. Lyu, L.; Niu, D.; Xie, H.; Cao, N.; Zhang, H.; Zhang, Y.; Liu, P.; Gao, Y., Orientation-dependent energy level alignment and film growth of 2,7-diocty[1]benzothieno[3,2-b]benzothiophene (C8-BTBT) on HOPG. *The Journal of Chemical Physics* **2016,** *144* (3), 034701.

40. He, D.; Zhang, Y.; Wu, Q.; Xu, R.; Nan, H.; Liu, J.; Yao, J.; Wang, Z.; Yuan, S.; Li, Y.; Shi, Y.; Wang, J.; Ni, Z.; He, L.; Miao, F.; Song, F.; Xu, H.; Watanabe, K.; Taniguchi, T.; Xu, J.-B.; Wang, X., Two-dimensional quasi-freestanding molecular crystals for high-performance organic field-effect transistors. *Nature Communications* **2014,** *5* (1), 5162.
41. Lyu, L.; Niu, D.; Xie, H.; Zhao, Y.; Cao, N.; Zhang, H.; Zhang, Y.; Liu, P.; Gao, Y., The correlations of the electronic structure and film growth of 2,7-diocty[1]benzothieno[3,2-b]benzothiophene (C8-BTBT) on SiO2. *Physical Chemistry Chemical Physics* **2017,** *19* (2), 1669-1676.
42. Kim, C. S.; Lee, S.; Gomez, E. D.; Anthony, J. E.; Loo, Y.-L., Solvent-dependent electrical characteristics and stability of organic thin-film transistors with drop cast bis(triisopropylsilylethynyl) pentacene. *Appl. Phys. Lett.* **2008,** *93* (10), 103302.
43. Kim, Y.-H.; Lee, Y. U.; Han, J.-I.; Han, S.-M.; Han, M.-K., Influence of Solvent on the Film Morphology, Crystallinity and Electrical Characteristics of Triisopropylsilyl Pentacene OTFTs. *J. Electrochem. Soc.* **2007,** *154* (12), H995.
44. Gbabode, G.; Dohr, M.; Niebel, C.; Balandier, J. Y.; Ruzie, C.; Negrier, P.; Mondieig, D.; Geerts, Y. H.; Resel, R.; Sferrazza, M., X-ray structural investigation of nonsymmetrically and symmetrically alkylated [1]benzothieno[3,2-b]benzothiophene derivatives in bulk and thin films. *ACS Appl Mater Interfaces* **2014,** *6* (16), 13413-21.
45. Dohr, M.; Werzer, O.; Shen, Q.; Salzmann, I.; Teichert, C.; Ruzié, C.; Schweicher, G.; Geerts, Y. H.; Sferrazza, M.; Resel, R., Dynamics of Monolayer–Island Transitions in 2,7-Dioctyl-benzothienobenzthiophene Thin Films. *ChemPhysChem* **2013,** *14* (11), 2554-2559.
46. Ebata, H.; Izawa, T.; Miyazaki, E.; Takimiya, K.; Ikeda, M.; Kuwabara, H.; Yui, T., Highly Soluble [1]Benzothieno[3,2-b]benzothiophene (BTBT) Derivatives for High-Performance, Solution-Processed Organic Field-Effect Transistors. *J. Am. Chem. Soc.* **2007,** *129* (51), 15732-15733.
47. Stöhr, J.; Outka, D. A., Determination of molecular orientations on surfaces from the angular dependence of near-edge x-ray-absorption fine-structure spectra. *Physical Review B* **1987,** *36* (15), 7891-7905.
48. Watanuki, H.; Mitsuhara, K.; Takizawa, M., Molecular Orientation Analysis of a C8-BTBT Thin Film Grown under an External Temperature Gradient. *e-Journal of Surface Science and Nanotechnology* **2018,** *16*, 79-83.
49. Kikuma, J.; Tonner, B. P., XANES spectra of a variety of widely used organic polymers at the C K-edge. *J. Electron. Spectrosc. Relat. Phenom.* **1996,** *82* (1), 53-60.
50. Stöhr, J., *NEXAFS spectroscopy*. Springer: New York, **1996**.
51. Mannebach, E. M.; Spalenka, J. W.; Johnson, P. S.; Cai, Z.; Himpsel, F. J.; Evans, P. G., High Hole Mobility and Thickness-Dependent Crystal Structure in α,ω-Dihexylsexithiophene Single-Monolayer Field-Effect Transistors. *Advanced Functional Materials* **2013,** *23* (5), 554-564.
52. Zheng, F.; Park, B.-N.; Seo, S.; Evans, P. G.; Himpsel, F. J., Orientation of pentacene molecules on SiO2: From a monolayer to the bulk. *The Journal of Chemical Physics* **2007,** *126* (15), 154702.
53. DeLongchamp, D. M.; Sambasivan, S.; Fischer, D. A.; Lin, E. K.; Chang, P.; Murphy, A. R.; Fréchet, J. M. J.; Subramanian, V., Direct Correlation of Organic Semiconductor Film Structure to Field-Effect Mobility. *Adv. Mater.* **2005,** *17* (19), 2340-2344.

54. Lei, T.; Wang, J.-Y.; Pei, J., Roles of Flexible Chains in Organic Semiconducting Materials. *Chem. Mater.* **2014,** *26* (1), 594-603.
55. Izawa, T.; Miyazaki, E.; Takimiya, K., Molecular Ordering of High-Performance Soluble Molecular Semiconductors and Re-evaluation of Their Field-Effect Transistor Characteristics. *Adv. Mater.* **2008,** *20* (18), 3388-3392.
56. Pérez-Rodríguez, A.; Temiño, I.; Ocal, C.; Mas-Torrent, M.; Barrena, E., Decoding the Vertical Phase Separation and Its Impact on C8-BTBT/PS Transistor Properties. *ACS Applied Materials & Interfaces* **2018,** *10* (8), 7296-7303.
57. Arnold, T.; Thomas, R. K.; Castro, M. A.; Clarke, S. M.; Messe, L.; Inaba, A., The crystalline structures of the even alkanes hexane, octane, decane, dodecane and tetradecane monolayers adsorbed on graphite at submonolayer coverages and from the liquid. *Physical Chemistry Chemical Physics* **2002,** *4* (2), 345-351.
58. Watanuki, H.; Mitsuhara, K.; Takizawa, M., Molecular Orientation Analysis of a C8-BTBT Thin Film Grown under an External Temperature Gradient. *e-Journal of Surface Science and Nanotechnology* **2018,** *16*, 79-83.

TOC Figure: